

Transport properties of ZrN superconducting films

A. Cassinese, M. Iavarone, and R. Vaglio

INFN–Dipartimento di Scienze Fisiche, Università di Napoli Federico II, Piazzale Tecchio 80, I-80125 Napoli, Italy

M. Grimsditch and S. Uran

Division of Materials Science, Argonne National Laboratory, Argonne, Illinois 60439

(Received 10 May 2000)

Superconductivity in nitrides presents intriguing aspects related to the role of optical phonons. In the present paper we report on high-quality superconducting zirconium nitride film preparation and characterization (including Raman scattering) as well as on both dc and microwave frequency transport properties. The high-temperature dc resistivity shows no evidence of saturation effects, possibly due to the low electron-phonon coupling. Surface impedance data can be well fitted by the standard BCS expressions. The data provide further evidence of the “conventional” nature of superconductivity in these compounds.

I. INTRODUCTION

The refractory NaCl (*B1*) type transition metal nitrides, characterized by the presence of an optical phonon branch well separated from the acoustic branch, have been widely studied in the past.¹ Though the basic features of superconductivity in these compounds appear to indicate a standard BCS mechanism, some points are still not fully clarified.

As an example, high quality tunneling spectroscopy experiments on ZrN (Ref. 2) clearly showed a typical BCS quasiparticle density of states. Data deconvolution using the McMillan and Rowel procedure³ gave the correct phonon locations and an almost constant electron-phonon coupling constant over the full spectrum. This was in contradiction with the theoretical prediction of a much higher (roughly a factor of 3) coupling of the electrons to the optical phonons than the acoustic ones in this material.⁴

As a second example the absolute value of the superconducting critical temperature T_c for VN can only be accounted for assuming strong spin fluctuation effects.^{4,5} However dc transport measurements, performed on high-quality VN thin films with controlled disorder,⁶ could only be partially reconciled with a BCS view if spin fluctuation effects were considered.

Recently, the “Uemura plot” is often used to discuss “conventional” versus “unconventional” superconductivity based on the location below or above an ideal separation line in a T_c vs γ plot, where γ is the Sommerfeld constant as obtained from specific heat data.⁷ In this picture oxide and organic superconductors are strong candidates for unconventional pairing mechanisms or symmetry, in contrast to cubic metallic elements or intermetallic compounds that are conventional (BCS) superconductors. Transition metal nitrides should also be unconventional in this view, since reported values of T_c and γ locate them well above the separation line.

To further clarify the nature of superconductivity in these compounds, we present here measurements of the dc and microwave transport in ZrN films fabricated by reactive magnetron sputtering. The observed absence of saturation in the high-temperature resistivity seems to support recent re-

sults based on dynamical mean field theory.⁸ The microwave surface impedance data confirm unambiguously the BCS, *s*-wave, and electron-phonon nature of superconductivity in transition metal nitrides.

II. FILM PREPARATION AND CHARACTERIZATION

ZrN films were prepared by a reactive magnetron sputtering technique starting from a two-inch diameter high purity (99.9%) Zr target. The substrates were placed “on axis” at 9 cm from the target surface and could be heated up to about 1000 °C by means of a molybdenum heater. Sapphire (Al_2O_3) substrates were used in this study. The base system pressure just before sputtering was in the low 10^{-6} Pa range. Titanium sublimation was used to lower the oxygen content. The film thickness was monitored during growth by a quartz oscillator. The final thickness was around 500 nm for all depositions. The Ar partial pressure was set to the value $P(\text{Ar})=6\times 10^{-1}$ Pa and the sputtering current to $I=1$ A. Keys to obtain high-quality films were the substrate temperature T_s and the nitrogen partial pressure $P(\text{N}_2)$. The best films were obtained for $T_s=900$ °C and $P(\text{N}_2)=5\times 10^{-1}$ Pa, corresponding to a growth rate of 0.6 nm/s.

The film showed a metallic-gold appearance. X-ray Θ -2 Θ diffraction patterns showed polycrystalline films with occasional preferential orientation along the (111) direction and a lattice parameter $a_0=0.45$ nm, close to the bulk value.

The transition temperature T_c and the critical current density J_c of the samples were measured using both standard four-probes and inductive methods. The optimized film transition temperature and residual resistivity ratio (RRR) at different substrate temperatures compare well with those reported in Ref. 9. The best films had $T_c=8.1$ K (onset of the resistive transition) and $\text{RRR}=1.6$. T_c and J_c were also evaluated inductively by measuring the first or the third harmonic component voltage across a small sensor coil mounted very close to the film surface, as a function of temperature and driving current, respectively.¹⁰ Measurements performed by this method on the best films, yielded $T_c=8$ K, $\Delta T_c=0.1$ K, and $J_c(0)=1.5$ MA/cm² (Fig. 1). From plots of T_c

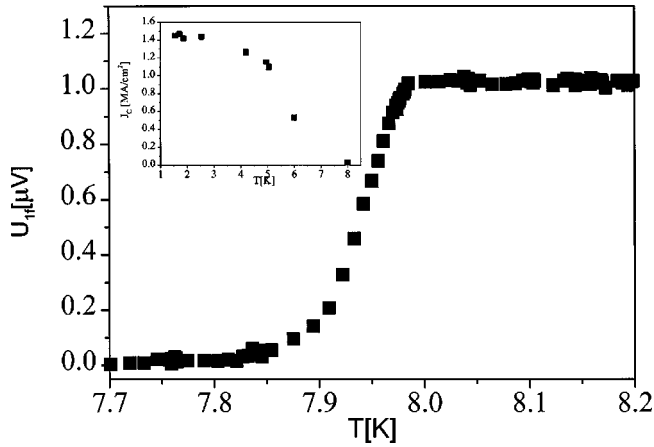


FIG. 1. First harmonic component of the coil voltage U_{1f} as a function of the temperature for a typical ZrN film. The inset shows the critical current density J_c , obtained by the same method as function of the temperature.

versus nitrogen content¹¹ we deduced a composition $\text{ZrN}_{0.97 \pm 0.01}$ for our films.

Because of the potential role played by the unusual distributions of phonons in these materials, we have also characterized our films using Raman spectroscopy. Figure 2 shows the Raman spectrum acquired from one of our films. Because of its structure, ZrN is not expected to produce any first order Raman lines and one expects to observe only broad spectral features due to second order (two-phonons) processes. However, due to the disorder induced by N vacancies, these crystals lose their translational invariance which in turn gives rise to a Raman spectrum reminiscent of a single phonon density of states. The features in Fig. 2 have been identified in Ref. 12. The peak in the $150\text{--}200\text{ cm}^{-1}$ range is associated with disorder induced single acoustic phonons, the shoulders at ≈ 330 and 400 cm^{-1} are due to second order (two acoustic phonons) processes, the peak at $\approx 500\text{ cm}^{-1}$ is due to disorder induced scattering from optic phonons and finally the feature at $\approx 670\text{ cm}^{-1}$ is associated with second order (acoustic+optic) scattering. All these features have frequencies in agreement with the Raman results reported in Ref. 12 and are consistent with the neutron scattering results¹³ and tunneling experiments.² In our spectrum the dis-

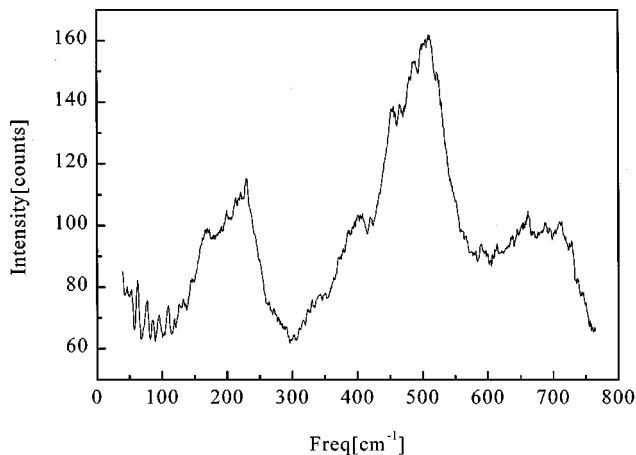


FIG. 2. Raman spectrum of a typical ZrN film.

order induced peaks are about a factor of two weaker than in Ref. 12. Since disorder induced scattering is likely to be proportional to the number of vacancies and the sample used in Ref. 12 was $\text{ZrN}_{0.95}$, this is consistent with the composition $\text{ZrN}_{0.97}$ independently estimated for our samples.

III. dc RESISTIVITY MEASUREMENTS

In Fig. 3 we show the dc resistivity as a function of the temperature for a typical optimized ZrN film. The absolute value of resistivity was determined at room temperature using a commercial linear four probe head (tip spacing = 0.65 mm). The absolute error, mainly associated with the thickness measurement performed by a standard profilometer, is estimated to be on the order of 5%. High-temperature data were taken using a four tungsten tip arrangement in flowing Ar, whereas low-temperature data were taken in a standard cryogenic holder.

Generally for metals the temperature dependence of the normal state resistivity is well described by the Mathiessen rule $\rho(T) = \rho_{\text{ph}}(T) + \rho_0$, where ρ_0 is related to impurities or defects and

$$\rho_{\text{ph}}(T) = (n-1)\rho' \theta_D \left(\frac{T}{\theta_D} \right)^n \int_0^{\theta_D/T} \frac{x^n dx}{(e^x - 1)(1 - e^{-x})} \quad (1a)$$

represents a generalized Bloch-Grüneisen expression for the electron-phonon contribution. In the limit $T \ll \theta_D$ ($T < 0.1\theta_D$) Eq. (1a) reduces to $\rho_{\text{ph}}(T) \propto T^n$, whereas for $T \gg \theta_D$ it is $\rho_{\text{ph}}(T) = \rho' T$.

In many cases for superconducting transition metals and alloys a high-temperature ‘‘saturation’’ of the resistivity occurs that can be described by a parallel resistor model

$$\rho^{-1}(T) = [\rho_{\text{ph}}(T) + \rho_0]^{-1} + \rho_s^{-1}, \quad (1b)$$

where ρ_s represents the ‘‘saturation value’’ related to the existence of a minimum value l_{min} for the mean free path.¹⁴ Since $\rho_0 \ll \rho_s$ one still has $\rho(0\text{ K}) = \rho_0$ so that ρ_0 can be always identified with the residual resistivity. This model successfully describes the high-temperature resistivity data for Nb, V, A15 compounds and for VN.¹⁵

As reported in Fig. 3, the resistivity data for our ZrN film can be well fitted by Eq. (1) with $\rho_0 = 40\text{ }\mu\Omega\text{ cm}$, $n = 5$, $\rho' = 0.105\text{ }\mu\Omega\text{ cm/K}$, $\theta_D = 415\text{ K}$, and assuming no saturation of the resistivity ($\rho_s^{-1} = 0$). The data show an upward curvature at $T > 550\text{ K}$, accompanied by an irreversible change of the resistance, indicating chemical modifications of the sample.

According to Gurwitch,¹⁶ the occurrence of a $n = 5$ exponent in the low-temperature resistivity data (Fig. 3, inset) would imply an upper limit $\lambda_{e\text{-ph}} \leq 1$ for the electron-phonon coupling constant. It is worth pointing out that VN, having a higher value of $\lambda_{e\text{-ph}}$, exhibits a lower power law exponent in the low-temperature resistivity.¹⁷ The value $\theta_D = 415\text{ K}$ obtained for the Debye temperature is significantly lower than estimates based on ultrasonic measurements (Ref. 11, $\theta_D = 600\text{ K}$). Our value is consistent with the Raman phonon frequency spectrum reported in Fig. 2 ($\langle \omega \rangle = 310\text{ cm}^{-1}, 38.4\text{ meV}, 445\text{ K}$). Inserting our θ_D value in the

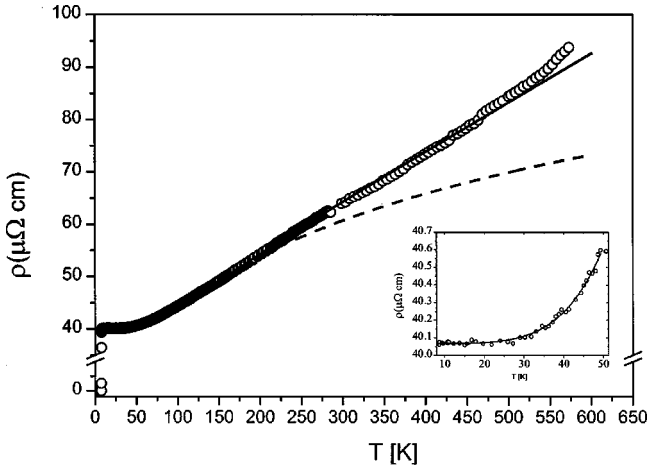


FIG. 3. Temperature dependence of the resistivity of a ZrN film. The continuous line represents the fit to the Block-Grüneisen formula (assuming no saturation effects). The dashed line is calculated by the parallel resistor model with $\rho_s = 110 \mu\Omega \text{ cm}$. In the inset the region $T < 50 \text{ K}$ is magnified.

classical MacMillan formula¹ and assuming the “standard” value $\mu^* = 0.1$ for the Coulomb pseudopotential, leads to $\lambda_{e\text{-ph}} = 0.61$ extremely close to the very accurate tunneling experiments by Geerk *et al.* (Ref. 2, $\lambda_{e\text{-ph}} = 0.62$). This confirms the prediction that, in ZrN, the effect of spin fluctuations is indeed negligible.⁴ It also confirms an almost constant electron phonon coupling constant α^2 , over both the acoustical and optical branches, as indicated by tunneling experiments² but in contrast with theoretical estimations.⁴

Assuming $\lambda_{tr} = \lambda_{e\text{-ph}}$ (Ref. 3) a plasma frequency $\omega_p = 4.9 \text{ eV}$ is found for ZrN through the relation¹⁴

$$\lambda_{tr} = 0.246 \omega_p^2 \rho'. \quad (2)$$

This value is very close to that previously found for VN.¹⁵ We can now estimate the expected saturation resistivity ρ_s by using the relation^{14,15}

$$\rho_s = \frac{4.95 \times 10^{-4} v_f}{\omega_p^2 l_{\min}}. \quad (3)$$

Assuming $l_{\min} = a_0 = 0.46 \text{ nm}$ (from x-ray measurements) and a “reasonable” value for the Fermi velocity $v_f = 2.4 \times 10^7 \text{ cm/s}$ (as evaluated for VN⁶) leads to $\rho_s = 110 \mu\Omega \text{ cm}$. The dashed curve in Fig. 3 is obtained inserting this value in Eqs. (1). A reasonable agreement with the data could only be achieved assuming an unrealistic value for v_f (over 10^8 cm/s). This clearly indicates the failure of the parallel resistor model to describe our ZrN data. Often, however, the validity of this approach has been questioned in the past. In particular in a recent paper a dynamical mean-field method was applied to study the high-temperature resistivity of metals with high electron-phonon coupling. The model does not predict a resistivity “saturation,” rather a change in the temperature dependence when scattering becomes sufficiently strong to cause a breakdown of the Migdal approximation.⁸ The calculations are in qualitative agreement with the experiments for strong coupling metals

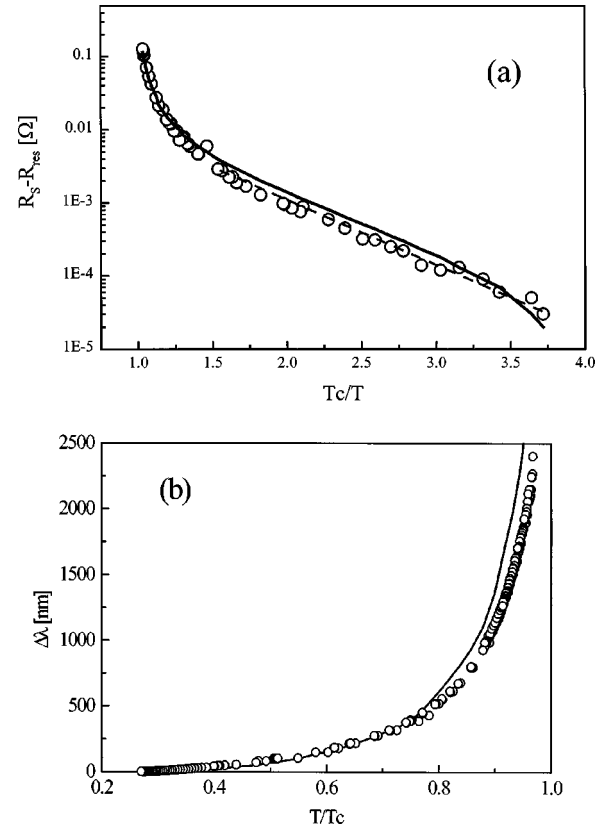


FIG. 4. (a) Surface resistance R_s (log scale) as a function of T_c/T . The dashed line underlines the exponential dependence at low temperatures. (b) Penetration depth changes $\Delta\lambda$ as a function of the reduced temperature T/T_c . The continuous lines in (a) and (b) represent the BCS fit.

($\lambda_{e\text{-ph}} > 1$) and predict no relevant deviation from linearity at high temperatures for weak coupling ($\lambda_{e\text{-ph}} \ll 1$) as observed in our case.

IV. SURFACE IMPEDANCE MEASUREMENTS

Microwave surface impedance measurements were performed using a dielectric resonator technique by a standard network analyzer. The dielectric resonator is entirely enclosed by a Cu box and makes use of two superconducting samples to shield the two end faces of a sapphire cylinder.

The quality factor is limited by conductor losses within the shield and by the loss tangent of the dielectric material used. The unloaded quality factor Q for the resonant system can be expressed as follows:

$$1/Q = R_s/A_{\text{sup}} + R_n/A_{\text{met}} + p_e \tan \delta,$$

where A_{sup} and A_{met} are geometrical factors for the conducting surfaces of the resonant system consisting of the superconducting material and the lateral copper shield respectively, R_s and R_n are the corresponding surface resistance values for superconductors and metal, p_e is the fraction of the electric energy stored in the dielectric material, and $\tan \delta$ is its dielectric tangent loss value. In our case a low-loss sapphire rod with a height $h = 3.5 \text{ mm}$ and a diameter D

=7 mm is used as a dielectric, yielding a fundamental resonant frequency at about 19 GHz, $A_{\text{sup}}=250\ \Omega$ and $A_{\text{met}}=2900\ \Omega$.

The shifts in the resonant frequency Δf are associated with the penetration depth changes $\Delta\lambda$ (related to changes in the surface impedance ΔX_s) through the relation

$$2\Delta f/f = \mu_0\omega(\Delta\lambda_{\text{sup}}/A_{\text{sup}} + \Delta\lambda_{\text{smet}}/A_{\text{met}}).$$

The input and the output coupling is achieved by open loop antennas connected to the microwave cables. The parasitic losses are mainly due to the copper walls, yielding a Q factor of about 4×10^4 with a sensitivity of $50\ \mu\Omega$.

To evaluate the surface resistance and changes in the penetration depth, one must perform at least two measurements: one with superconducting films and the other one replacing the superconductors by metal plates made of the same material as the lateral surface. Calibration measurements performed with Cu samples gave, at temperatures of our interest ($T < 20\ \text{K}$), $R_{s\text{Cu}}=1.5\ \text{m}\Omega$ and $\Delta\lambda_{\text{Cu}}\approx 0$.

Typical measurements of the surface resistance and of the penetration depth are reported in Figs. 4(a) and 4(b), respectively. The exponential dependence on the inverse of the temperature, characteristic of an activated behavior over a constant energy gap, is clearly exhibited. The continuous lines represent the BCS fit obtained with the HALBRITTER code¹⁸ with $\xi_0=40\ \text{nm}$ and $l=1.2\ \text{nm}$ (estimated assuming $v_F=2.4\times 10^7\ \text{cm/s}$ as discussed above; the fitting quality is not affected by the precise choice of these values).

The possibility of accurately fitting both R_s and λ values simultaneous (i.e., the full complex surface impedance) fully confirms the BCS s -wave nature of superconductivity in

ZrN. The value of $2\Delta/K_B T_c=3.9$ is slightly higher than the tunneling estimates (Ref. 3, $2\Delta/K_B T_c=3.7$) and a little above the weak coupling BCS prediction. The high value found for the penetration depth $\lambda(0)=1400\ \text{nm}$ may be due to the granular nature of the samples.¹⁹

V. CONCLUSIONS

In the present paper we have discussed the properties of sputter-deposited high-quality ZrN films. The resistivity measurements show that ZrN is a conventional metal ($\text{RRR}=1.6$) with normal state transport properties dominated by electron phonon scattering. The T^5 power law dependence observed at low temperatures is compatible with the estimated value of the electron-phonon constant ($\lambda_{e\text{-ph}}=0.61$). The data also support the tunneling evidence of a constant α^2 value over both the acoustical and optical branches. Moreover the film resistivity does not show any saturation at high temperatures. This agrees with a recent model that instead of saturation predicts a change in the temperature dependence when scattering becomes sufficiently strong to cause a breakdown of the Migdal approximation.⁸

Microwave measurements are well described by the standard BCS expressions indicating s -wave superconductivity. The fitting parameters yield a value of $2\Delta/K_B T_c=3.9$, slightly higher than previous tunneling estimates (Ref. 3, $2\Delta/K_B T_c=3.7$).

ACKNOWLEDGMENTS

The authors wish to thank L. Gianni for help in the measurements. The technical support of A. Maggio and S. Marrazzo is acknowledged. Work at ANL was supported by the U.S. DOE BES under Contract No. W-31-109-Eng-38.

¹S. V. Vonzovski, Yu. A. Izyumov, and E. K. Kurmaev, *Superconductivity of Transition Metals* (Springer-Verlag, Berlin, 1982).

²J. Geerk, G. Linker, and R. Smithey, Phys. Rev. Lett. **57**, 3284 (1986).

³E. L. Wolf, *Principles of Electron Tunneling Spectroscopy* (Oxford University Press, Oxford, 1985).

⁴H. Rietshel, H. Winter, and W. Reichardt, Phys. Rev. B **22**, 4284 (1980).

⁵H. Rietshel and H. Winter, Phys. Rev. Lett. **43**, 1256 (1979).

⁶K. E. Gray, R. T. Kampwirth, D. W. Capone II, R. Vaglio, and J. Zasadzinski, Phys. Rev. B **38**, 2333 (1988).

⁷Y. J. Uemura, Phys. Rev. Lett. **66**, 2665 (1991).

⁸A. J. Millis, Jun Hu, and S. Das Sarma, Phys. Rev. Lett. **82**, 2354 (1999).

⁹V. M. Pan, V. A. Komashko, E. M. Rudenko, Y. M. Bogoslavsky, and L. Zelenkevich, IEEE Trans. Magn. **MAG-23**,

1436 (1987).

¹⁰J. H. Classen, M. E. Reeves, and R. J. Soulen, Rev. Sci. Instrum. **62**, 996 (1991).

¹¹T. Wolf, Ph.D. thesis, University of Karlsruhe, 1982.

¹²W. Spengler and R. Kaiser, Solid State Commun. **18**, 881 (1976).

¹³A. N. Christensen, O. W. Dietrich, W. Kress, and W. D. Teuchert, Phys. Rev. B **19**, 5699 (1979).

¹⁴M. Gurvitch, Phys. Rev. B **34**, 540 (1986).

¹⁵N. Tralshawala, J. F. Zasadzinski, L. Coffey, W. Gai, M. Romalis, Q. Huang, R. Vaglio, and K. E. Gray, Phys. Rev. B **51**, 3812 (1995).

¹⁶M. Gurvitch, Physica B & C **135B**, 276 (1985).

¹⁷J. F. Zasadzinski, A. Saggese, K. E. Gray, R. T. Kampwirth, and R. Vaglio, Phys. Rev. B **38**, 5065 (1988).

¹⁸J. Halbritter, Z. Phys. **266**, 209 (1974).

¹⁹T. Hylton, A. Kapitulnik, M. R. Beasley, J. P. Carini, L. Drabek, and G. Gruner, Appl. Phys. Lett. **53**, 1343 (1988).